Bloch-Wave Analysis in Electron Diffraction Experiments with a CaF_2 Single-Crystal Wedge

K. Ishida [+], A. W. S. Johnson [++], and G. Lehmpfuhl [*]

Fritz-Haber-Institut der Max-Planck-Gesellschaft, W.-Berlin

[+] College of General Education, University of Tokyo, Komaba, Meguro-ku, Tokyo, Japan.
[++] C.S.I.R.O., Division of Chemical Physics, Melbourne, Australia.

(Z. Naturforsch. **30 a**, 1715—1729 [1975]; received November 12, 1975)

The fine-structure spots in an electron diffraction pattern from a crystal wedge represent the strong partial waves of strongly excited Bloch waves. Diffraction experiments near the [100] and the [110] zone axes of a CaF_2 crystal were carried out in order to determine from a fine-structure profile analysis the low-indexed structure potentials V_{111}, V_{200} and V_{220} and the absorption coefficients of different Bloch waves. Under these experimental conditions there exist three strong Bloch waves; one is concentrated at the rows of Ca atoms, another along the rows of F atoms and a third is concentrated in the space between the atom rows. The absorption coefficients depend in a characteristic way on the density of atoms along the atom rows. This density is different for the two projections leading to different absorption coefficients. A strong background due to inelastic scattering was observed mainly in one strong reflection which was supposed to be due to phonon excitation.

The distribution of electrons travelling through a single crystal can be described by the Bloch-wave picture. Near low-indexed zone axes the different Bloch waves show characteristic density distributions. They contain information on elastic and inelastic interactions with the crystal. The possibility of a direct analysis of these Bloch waves in electron diffraction experiments with a single-crystal wedge was shown in previous papers [1, 2, 3]. In such diffraction experiments the Bloch waves are dispersed into their partial waves and the strong ones can be identified in the reflections as fine-structure spots representing points on the dispersion surface.

In this paper we want to report on investigations of Bloch waves in CaF_2. In CaF_2 there exist various directions along which the atom strings consist of only one kind of atoms. For different directions the density of atoms along the strings is different which is of great interest with respect to elastic and inelastic scattering. In the same way as for MgO, macroscopic wedges of CaF_2 can be produced by cleavage.

§ 1. CaF_2 Crystal

The CaF_2 lattice is built up by one fcc lattice of Ca atoms and two fcc lattices of F atoms shifted along the diagonal by $\pm 1/4(a_1+a_2+a_3)$ with respect to the lattice of the Ca atoms. The investigations were done with macroscopic crystal wedges which were produced by cleavage. Generally the cleavage faces are (111) faces. Sometimes (112) faces were produced. Two possible wedges can be produced by (111) planes which are shown in Figure 1. In the experiment with the 109° wedge the direction of the incident electrons was near [001] and with the 71° wedge near [110]. These are two characteristic zone axes for which the atoms of only one kind are lying along strings. Figure 2 a shows the atoms projected on the (001) plane for the 109° wedge and Fig. 2 b on the (110) plane for

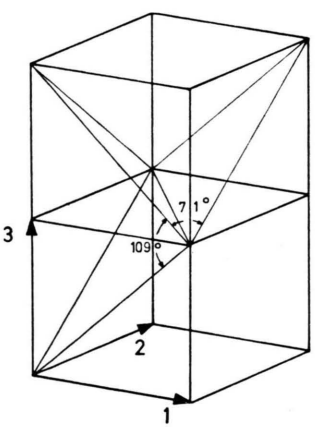

Fig. 1. Cubic lattice with two (111) planes producing two wedges; one with a 71° wedge angle and another with a 109° wedge angle.

Reprint requests to Dr. G. Lehmpfuhl, Abt. Prof. Dr. K. Molière, Fritz-Haber-Institut, *D-1000 Berlin*, Faradayweg 4—6.
* Abt. Prof. Dr. K. Molière.

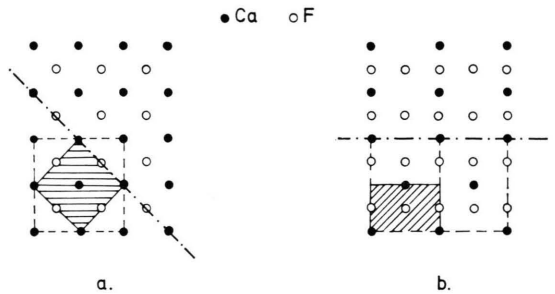

Fig. 2 a and b. Projection of the atoms of a CaF_2 crystal on the (100) plane (a) and on the (110) plane (b). The projection of the primitive cube is indicated by dashed lines; the projection of the edge is indicated by the dash-dotted lines. The electron-density distribution in the Bloch waves was calculated for the hatched areas.

the 71° wedge. The direction of the edge and the projection of the unit-cell cube are indicated by the dot-dashed and the dashed lines respectively.

The density of atom strings in the projected area is different for Figs. 2 a and 2 b. Under the condition for the sharp wedge experiment (Fig. 2 b) we have less Ca-atom strings and more F-atom strings than for the blunt-wedge experiment (Figure 2 a). Consequently the density of atoms along the strings is different in the two cases.

§ 1.1. The 109° Wedge

The blunt wedge was produced by a (111) and a $(11\bar{1})$ cleavage plane. The edge was parallel to $[\bar{2}20]$. The (111) face was the entrance surface for the electron beam. Diffraction patterns, taken with the incident beam near the [001] zone axis, showed many reflections with several fine-structure spots. Three slightly different excitation conditions were investigated. In Fig. 3 a the (001) plane of the reciprocal lattice is shown with three different intersection circles with the Ewald sphere indicating three slightly different excitations. Circle (1) belongs to an orientation where 220, 200 and 020 are simultaneously excited. The excitation conditions are determined by the intersection points of the Ewald sphere with the [220] axis called G and with the $[\bar{2}20]$ axis called H. The unit of these parameters is the length of the reciprocal vector [110]. That means e.g. if $G=2$ the Ewald sphere intersects the [110] axis at the reciprocal lattice point 220. The three orientations are characterized by the following pairs of G and H:

(1) $G=2$, $H=0$; (2) $G=0$, $H=2$;
(3) $G=-2$, $H=0$.

In the experiments small deviations from these orientations occured.

§ 1.2. The 71° Wedge

The sharp wedge was produced by a $(1\bar{1}\bar{1})$ and a $(\bar{1}1\bar{1})$ cleavage plane. The edge was parallel to [220]. Diffraction patterns were taken near the $[1\bar{1}0]$ zone axis for two different orientations shown in Fig. 3 b by the two intersection circles (1) and (2) of the Ewald sphere with the $(\bar{1}10)$ plane of the reciprocal lattice. The two orientations are again characterized by the pairs of G and H:

(1) $G=-2$, $H=0$; (2) $G=0$, $H=2$.

§ 2. Experiment

The experiments were performed in a similar way as described earlier [1, 2]. The crystal was mount-

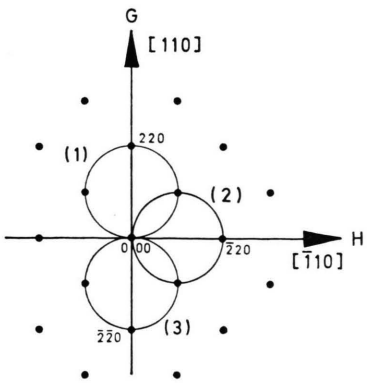

Fig. 3 a

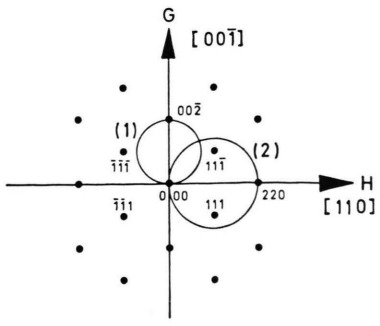

Fig. 3 b

Fig. 3 a and b. (001) plane (a) and $(\bar{1}10)$ plane (b) of the reciprocal lattice. The intersection circles of the Ewald sphere with these planes are indicated for three different directions of incidence (1), (2) and (3) in (a) and for two different directions of incidence (1) and (2) in (b). These orientations are characterized by two parameters G and H, which are the intersection points of the Ewald sphere with the [110] and the $[\bar{1}10]$ axes in Fig. 3 a resp. and with the [001] and the [110] axes in Fig. 3 b resp. For $G=0$ and $H=2$ in (a) the Ewald sphere intersects only the $[\bar{1}10]$ axis at the reciprocal lattice point $\bar{2}20$, and in (b) the [110] axis at 220.

ed on a goniometer stage and oriented with respect to the direction of the incident electron beam by looking at the Kikuchi pattern. Such a Kikuchi pattern obtained by focussing the beam at the crystal edge is shown in Figure 4. * Many reflections can be seen. The quality of the edge was checked by looking at its shadow image in the strong excited reflections as well as in other weak reflections. Each of the reflections shows a fine structure which can be seen much more clearly by focussing the electron beam on the photographic plate. Instead of taking sections through the dispersion surface by the rotating crystal method the crystal was kept in a fixed position. In order to improve the signal to noise ratio in photometry curves the diffraction pattern was scanned over the photographic plate by means of a deflecting field. The diffraction spots are thereby elongated to streaks in a direction perpendicular to their splitting (see Figure 6). *

The fine structures were analysed for the 11 inner reflections (the zero beam was excluded). Because of the large intensity ratio between the strong and the weak reflections exposure series were taken with ratios up to 1 : 20. The photographs were taken on ILFORD NE4.50 films (as in earlier experiments [4]) which were developed in ILFORD ID 2 giving an exact linear dependence of density to electron intensity up to a density of $D \approx 1.6$. A density of 0.1 is produced by $\sim 3.5 \cdot 10^7$ electrons/cm^2 which corresponds to 315 electrons on an area of $30 \times 30\,\mu^2$. $30\,\mu$ is approximately the point resolution of the film.

Initially the direction of the incident beam could only be estimated from the Kikuchi diagram in Figure 4. This is due to the fact that the fine-structure spots do not directly indicate an exact relation to the geometry of the reciprocal lattice and that the Kikuchi-line profiles are broad and have small contrast. A more precise determination of the orientation was possible during the analysis by comparison of the experiment with a series of many-beam calculations. These calculations were performed near the estimated orientation in steps ΔH and ΔG of 0.025.

§ 3. Theory

Coherent Superposition of Fine-Structure Spots

The analysis of the Bloch waves was done by fitting the photometer curves of the diffraction spots shown in Fig. 6 with calculated intensity distributions. The partial-wave amplitudes $\psi_g^{(i)}$ of the Bloch waves (i) and their wave vectors $k_g^{(i)}$ were calculated by solving an eigenvalue problem as described in a previous paper [1].

In the crystal each Bloch wave is absorbed with its own characteristic absorption coefficient μ_i as was predicted by v. Laue [5]. Due to this absorption a Bloch wave (i) decays with increasing distance from the entrance surface. Consequently each partial wave of this Bloch wave decays with the same absorption coefficient μ_i. In the diffraction pattern one observes the Fourier transform of the amplitude distribution at the exit surface. The damping of the amplitudes at the exit surface results in a broadening of the corresponding fine-structure spots as was shown earlier [6].

On the exit surface the Bloch wave (i) has the following form (see appendix)

$$\psi_i(r) = \exp\left\{-\frac{\mu_{is}}{2}\,t\right\} \sum_g \psi_g^{(i)} \exp\left\{\frac{2\pi i}{\lambda} \cdot \mathbf{S}_g^{(i)} \cdot \boldsymbol{r}\right\}. \tag{1}$$

$\psi_g^{(i)}$ is the partial-wave amplitude, $\mathbf{S}_g^{(i)}$ the corresponding reduced wave vector, λ the vacuum wave length of the primary electrons, μ_{is} the absorption coefficient of Bloch wave (i) on the exit surface, $\boldsymbol{r}$ a point on the exit surface and t its distance from the edge (see Figure 5). In a diffraction spot g one observes the Fourier transform of the amplitude distribution of the corresponding term of (1) as a

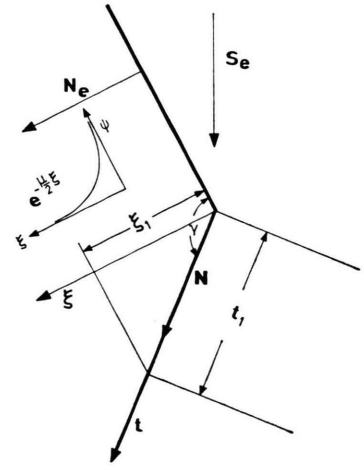

Fig. 5. Schematic diagram for the explanation of the absorption of Bloch waves with increasing distance from the entrance surface. $\boldsymbol{N}_e$ is a unit vector perpendicular to the entrance surface, $\boldsymbol{S}_e$ is the direction of the primary beam and $\boldsymbol{N}$ a unit vector in the exit surface perpendicular to the edge. From $\xi_1 = t_1 \sin\gamma$ and $\exp\{-\mu(\xi_1/2)\} = \exp\{-\mu_s(t_1/2)\}$ follows that $\mu \sin\gamma = \mu_s$.

* Figures 4, 6 and 15 on p. 1718 a, b.

fine-structure spot. This Fourier transform is given by the Kirchhoff integral

$$U_g^{(i)}(\boldsymbol{S}) = \psi_g^{(i)} \cdot \int_0^\infty \exp\left\{\frac{2\pi i}{\lambda}\left[(\boldsymbol{S}_g^{(i)} - \boldsymbol{S})\,\boldsymbol{N}\,t + i\,\mu_{is}\frac{\lambda}{4\pi}\,t\right]\right\} \mathrm{d}t\,. \tag{2}$$

$\boldsymbol{S}$ is a unit vector in the direction of observation and $\boldsymbol{N}$ a unit vector in the exit surface perpendicular to the edge. The result of integration gives

$$U_g^{(i)}(\boldsymbol{S}) = C \cdot \frac{\psi_g^{(i)}}{(\boldsymbol{S}_g^{(i)} - \boldsymbol{S})\cdot\boldsymbol{N} + i\,\mu_{is}\,\lambda/4\pi}\,. \tag{3}$$

$|\boldsymbol{U}_g^{(i)}(\boldsymbol{S})|^2$ describes the intensity distribution of one fine-structure spot belonging to Bloch wave (i) in the reflection g. Due to the existence of many strong Bloch waves we have to consider in one reflection g the coherent superposition of such distributions. The coherent overlapping of the fine-structure spots was shown at first by Didszuhn [8]. The total distribution has the form

$$U_g(\boldsymbol{S}) = C \cdot \sum_i \frac{\psi_g^{(i)}}{(\boldsymbol{S}_g^{(i)} - \boldsymbol{S})\cdot\boldsymbol{N} + i\,\mu_{is}\,\lambda/4\pi}\,. \tag{4}$$

Introducing the eigenvalues τ_i' [see (5) appendix] in (4) one obtains

$$U_g(\boldsymbol{S}) = C \cdot \frac{\lambda}{2\pi}\sum \psi_g^{(i)} \left\{(\boldsymbol{S}_e + \boldsymbol{B}_g - S)\,\boldsymbol{N} + \tau_i'\,\boldsymbol{N}_e\,\boldsymbol{N} + i\,\mu_{is}\,\lambda/4\pi\right\}. \tag{5}$$

The intensity distribution in the reflection g is then given by

$$\sum_i I_g(\boldsymbol{S}) = U_g(\boldsymbol{S})\cdot U_g^*(\boldsymbol{S})\,. \tag{6}$$

($\boldsymbol{S}$ means the direction of observation as mentioned above.) The intensity profile for the reflection g is expressed in this way by the eigenvalue τ_i' and the amplitudes $\psi_g^{(i)}$ of the eigenvectors obtained from a many-beam calculation. The absorption coefficients μ_{is} were determined by comparison with the experiment by trial and error. For the blunt wedge we had to consider the superposition of up to 9 partial waves and for the sharp wedge the superposition of 14 – 15 partial waves in the weak reflections.

§ 4. Results

a) 109° Wedge

The fine-structure profiles were analysed for the direction of incidence given by $G = 2$, $H = 0$ which is shown in Fig. 3 a as circle (1). The reflections of a diffraction pattern taken at that orientation show the fine structure very clearly as one can see in Figure 6. The spots are elongated to streaks perpendicular to the direction of splitting by applying the deflecting field as mentioned above. The 220 reflection was taken by a particularly short exposure. In the different reflections partial waves of individual Bloch waves numbered from the bottom to the top can be recognized. They are numbered in the order of the magnitude of the eigenvalues (Humphreys et al. [14]). In some reflections up to 6 separate streaks are identified.

For an orientation $H = 0$ the fine-structure profiles should be identical in the pairs (240, 420), (040, 400) etc. This criterion is a help for adjusting the crystal and for determining the orientation in connection with calculations. The profiles of reflections very near to the zero beam as 220, 200 and 020 are not so strongly orientation dependent as the outermost reflections.

The separation of the three strong fine-structure spots in the 220 reflection of Fig. 6 was compared with a calculated intensity profile [Eqs. (5) and (6)] using eigenvalues τ_i' and partial wave amplitudes $\psi_g^{(i)}$ which were determined by a 50-beam calculation. The accuracy of this approximation was tested with an 88-beam calculation for the purpose of proving the convergence of eigenvalues and eigenvectors. The difference between the two approximations was less than 1%.

The structure potentials V_{200} and V_{220} were used as adjustable parameters while the higher-order values were calculated from atomic scattering factors due to Doyle and Turner [9] for neutral Ca and F. This procedure was justified since the ionic state has only an influence on the low-order structure potentials V_{111}, V_{200} and V_{220} as was discussed earlier [2]. The assumption that the higher-order structure potentials are known with sufficient accuracy implies the knowledge of a correct Debye-Waller factor. The most reliable values given by Maslen [10] were used, with $B_{Ca} = 0.6$ and $B_F = 0.8$.

The three eigenvalues of Bloch waves (1), (2) and (3) depend in a characteristic way on the structure potentials V_{200} and V_{220} as shown in Fig. 7 a and b. We see that it is possible to determine V_{200} and V_{220} simultaneously by fitting the calculation with the experiment. The determination of the structure potentials V_{200} and V_{220} was independent from

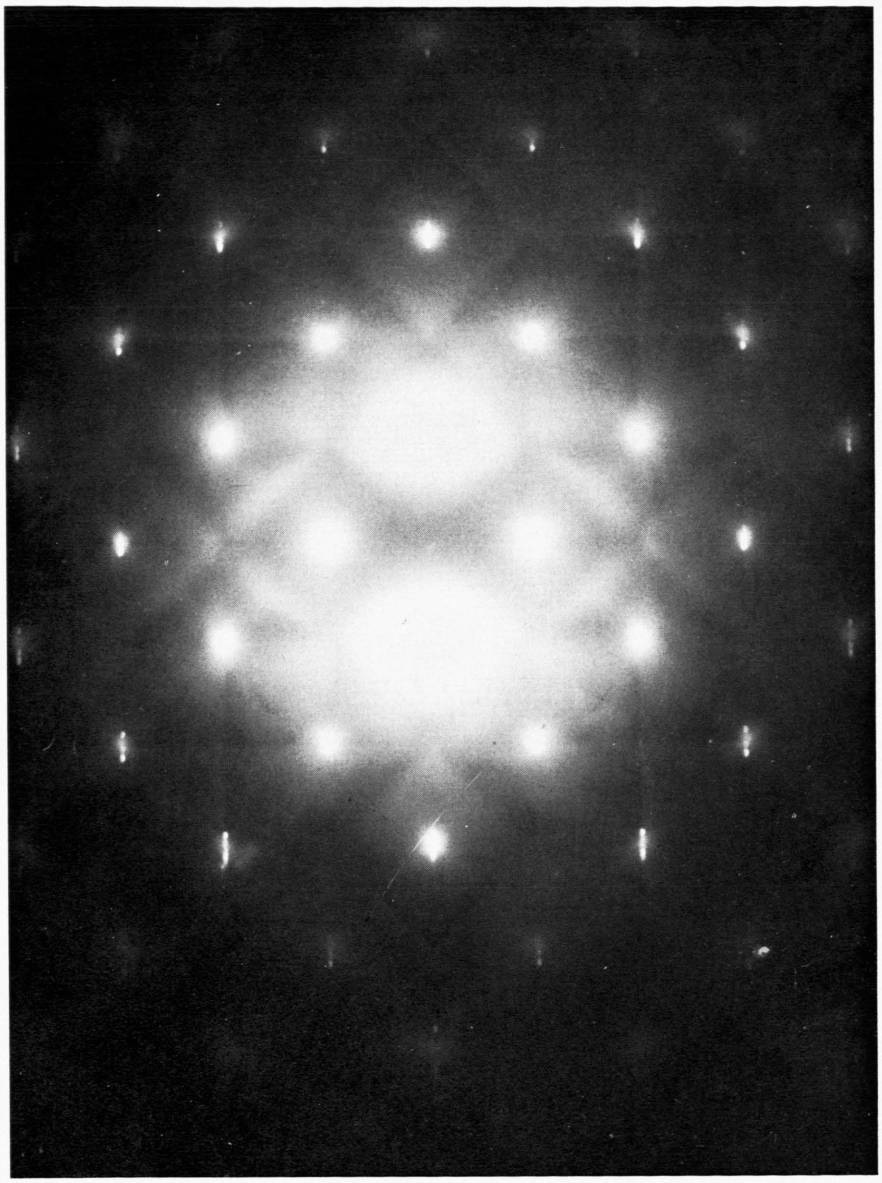

Fig. 4. Kikuchi pattern from a CaF_2 blunt-wedge crystal near the [001] zone axis at $G=2$ and $H=0$ [condition (1) in Figure 3 a].

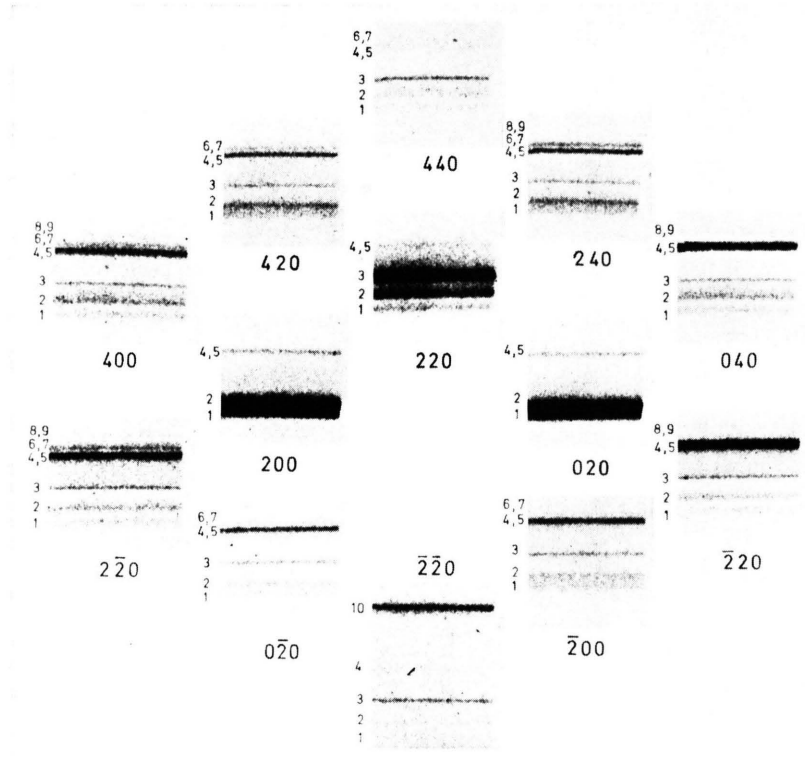

Fig. 6. Fine structure in the diffraction spots of CaF_2 near the [001] zone axis at $G=1.975$ and $H=0.025$. By a deflection perpendicular to the direction of splitting, the fine-structure spots are elongated into streaks to improve the signal-to-noise ratio. The 220 reflection in this picture was taken from a photographic record of shorter exposure time. The Bloch waves are numbered from the bottom to the top according to the magnitude of their eigenvalues. Bloch wave (1) has the largest eigenvalue (109° wedge, 60 keV electrons, condition (1) in Figure 3 a).

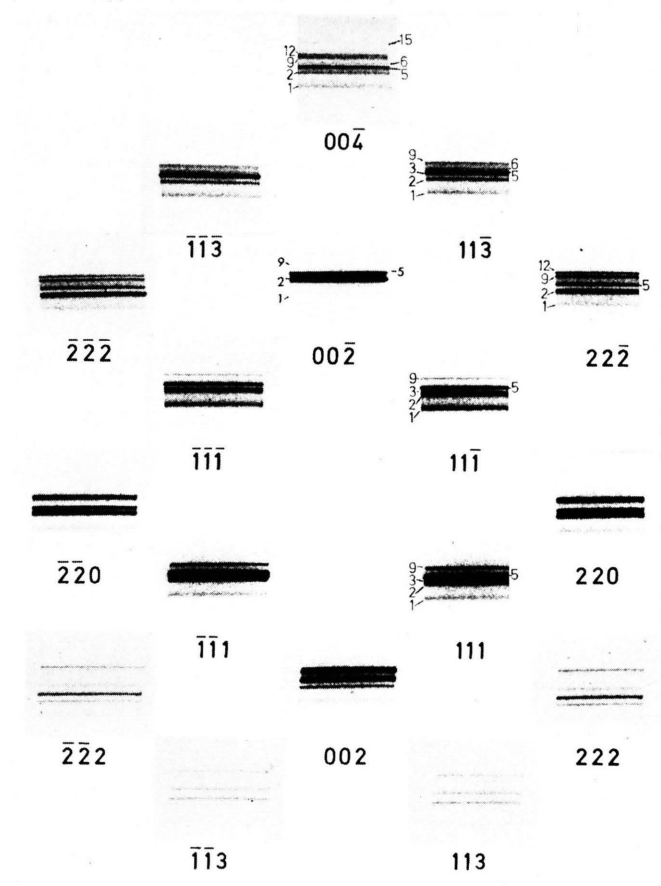

Fig. 15. Fine structure in the diffraction spots near the [110] zone axis at $G=-1.75$ and $H=0.0$. In some reflections the Bloch waves are numbered as in Fig. 6 [condition (1) in Fig. 3 b, 71° wedge, 60 keV electrons].

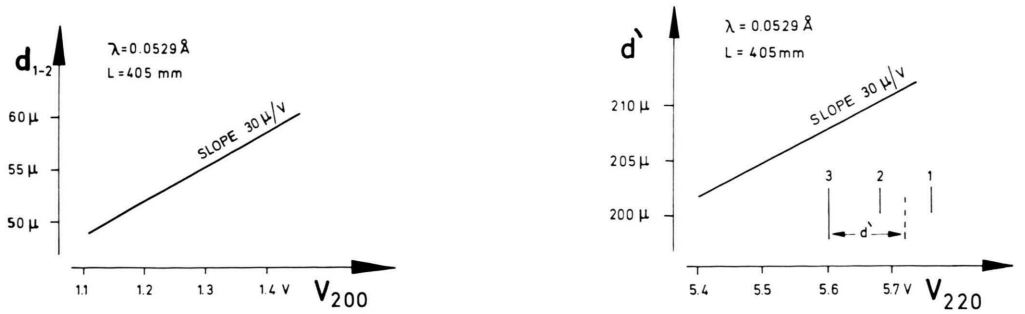

Fig. 7 a and b. Dependence of the eigenvalue differences d_{1-2} and d' on the structure potentials V_{200} and V_{220} for the three strong Bloch waves indicated in (b) ($G=2$, $H=0$, blunt wedge, L=camera length).

that of the structure potentials V_{111}. This value was determined by the experiment with the sharp wedge.

During the analysis it was found that the low-indexed structure potentials could not be determined independently from the absorption coefficients of the three Bloch waves. These can be estimated by looking at the electron density of the Bloch waves, as it was shown in Reference 3. The electron density distribution in the strong Bloch waves projected on the (001) plane for the orientation $G=2$, $H=0$ is plotted in Figure 8. The area for which the density distribution was calculated is indicated in Figure 2 a. From Fig. 8 we see that Bloch wave (1) has density maxima at the projections of the Ca atoms, that means at the rows of Ca atoms, Bloch wave (2) is concentrated at the rows of F atoms while Bloch wave (3) travels between the atomic rows etc. From such a picture relations between the absorption coefficients can be estimated.

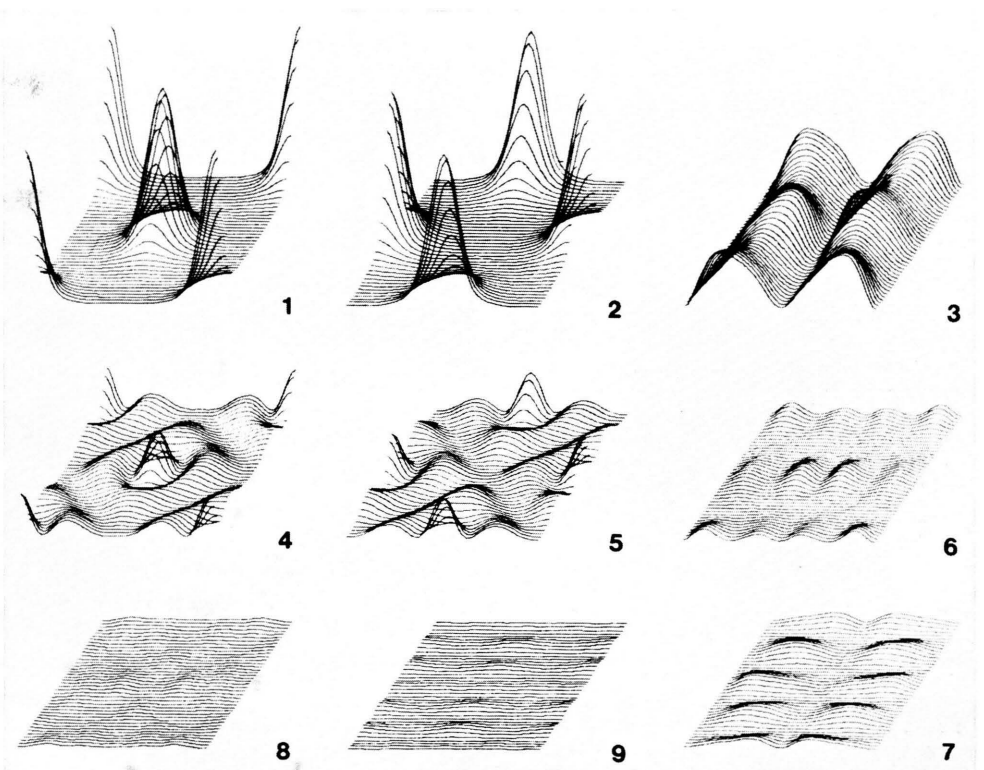

Fig. 8. Electron density distribution in the strong Bloch waves for $G=2$ and $H=0$ near the [001] zone axis. The density distribution was calculated for the hatched area in Fig. 2 a by a 42-beam approximation.

The three fine-structure spots in 220 of Fig. 6 belong to the three Bloch waves (1), (2) and (3). Also in all other weak reflections these Bloch waves can be identified. It is interesting to see that Bloch wave (3) has no 200 and 020 Fourier components (partial waves).

From Fig. 8 it is clear that Bloch wave (1) which is concentrated at the rows of Ca atoms must be absorbed most strongly while Bloch wave (3) encounters the smallest absorption. This results in a broad and low peak of the fine-structure spots representing Bloch wave (1) in the different reflections of Fig. 6 and a relatively sharp and high peak due to Bloch wave (3). The absorption coefficients for these three Bloch waves were estimated from the analysis of the reflections 220, 200 and 020 applying Eqs. (5) and (6). With these values the structure potentials V_{200} and V_{220} could be determined from the 220 profile by trial and error.

The comparison between experiment and calculation giving the best fit is shown in Figure 9. It is remarkable that the distance between the fine-structure maxima (1) and (2) in the 220 reflection is different from the corresponding distance in the 020 and 200 reflections. Also the shape of that part of the intensity distribution in 220 which is due to the Bloch waves (1) and (2) is different from the corresponding distribution in 200 and 020. This fact is due to the influence of the sign of the partial-wave amplitudes in coherent overlapping of broadened peaks according to Eqs. (5) and (6). In the (220) reflection the partial waves (1) and (2) have the same signs, whereas they have the opposite sign in (200) and (020).

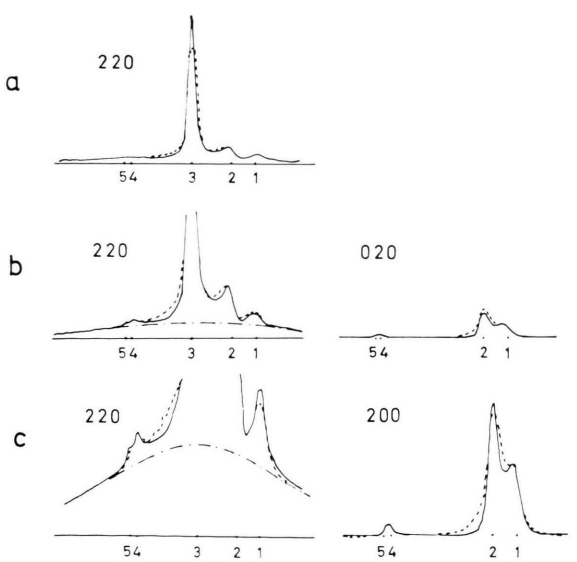

Fig. 9. Comparison of calculated fine-structure profiles (solid curve) with photometer records of the diffraction pattern (dashed curves) for an orientation of the blunt wedge near $G=1.975$ and $H=0.025$ (condition (1) in Figure 3 a). In the 220 reflection a background was taken into account, which can be seen clearly in the different exposures in a, b and c. The exposure time ratio was 1:3.3:19. In 200 and in 020 there is no strong background (109° wedge, 60.85 keV electrons). The background is indicated by the dash-dotted lines.

The strong excited (220) reflection in Fig. 9 shows experimentally a strong background which is due to inelastic processes. This background was fitted by assuming a Gaussian distribution [15]

$$A \cdot \exp\left\{\frac{-(\Delta\Theta+\alpha)^2}{\beta^2}\right\}$$

which was found to be equal for the three experimental conditions (1), (2) and (3) indicated in Fig. 3 a. It is most interesting to see that this background is connected with the existence of a strong partial wave of Bloch wave (3) in the reflection. In the reflections 200 and 020 there is not such a background. This result will be discussed later in a separate paper [16].

The comparison of experimental curves with intensity profile calculations due to Eq. (5) for the weak reflections is shown in Figure 10. The exact orientation characterized by G and H, the structure potentials V_{200} and V_{220} and the absorption coefficients of 9 Bloch waves were adjusted to give the best consistent fit. No background was considered in the weak reflections. During this procedure the structure potentials V_{200} and V_{220} could be refined since the difference between the eigenvalue pair (4), (5) and the eigenvalue pair (1), (2) depends on these structure potentials, that is, the distance between fine-structure spots (1), (2) and (4), (5) which can be measured very accurately in the weak beams as e.g. in 040 in Figure 10.

The agreement between calculation and experiment in Fig. 10 is quite reasonable. Deviations may be due to incorrect orientations, slightly wrong structure potentials and absorption coefficients, distortion of the crystal as defects, missing edge, distortion of the surface etc., neglected background due to inelastic processes and influence of many-beam effects, not taken into account in the 50-beam approximation.

We can see the degree of accuracy by comparing the results for $G=1.975$, $H=0.025$; $G=-0.05$,

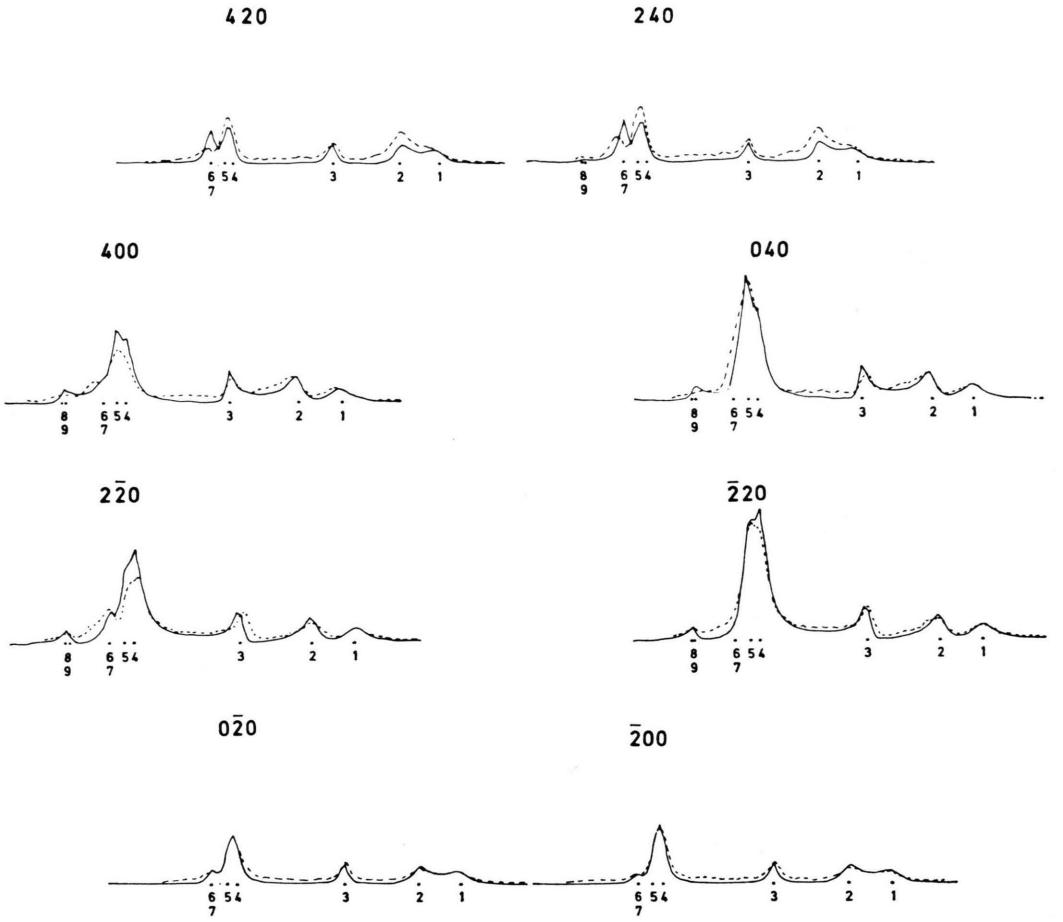

Fig. 10. Comparison of calculated intensity distributions (———) with photometer records (— — —) of the weak reflections of Figure 6. (G=1.975, H=0.025, 109° wedge, 60.85 keV electrons).

$H = 2.0$ and $G = -2.025$, $H = 0.025$ in Figs. 10, 11 and 12 corresponding respectively to circle (1), (2) and (3) in Figure 3 a. In the calculations the same absorption coefficients and the same structure potentials were used. Influence of neglected background can be seen in $\bar{2}\bar{2}0$ and $\bar{4}00$ of Figure 11. Another characteristic deviation was found in 420 and 240 of Fig. 10, where the calculated Bloch wave (2) is too weak, while in $\bar{2}\bar{4}0$ and $\bar{4}\bar{2}0$ of Fig. 12 Bloch wave (2) is too strong. It was not possible to overcome this disagreement by changing the orientation in the calculation.

In the diffraction pattern one can observe a symmetry with respect to the ($\bar{1}$10) plane if $H = 0$. The reflections 420 and 240 in Figs. 6 and 10 e.g. would then be identical. Their partial waves would have the same amplitude and the same sign. From the observation of symmetry one can estimate if $H = 0$ or not. The deviation from symmetry in the pairs (420, 240), (400, 040) etc. and (200, 020), ($2\bar{2}0$, $\bar{2}20$) etc. of Fig. 10 and Fig. 12, respectively, allows an estimate of the value of H. The corresponding symmetry for $G = 0$ with respect to the (110) plane is distorted because of the inclination of the entrance surface to the (110) mirror plane. For $G = 2$ there is a symmetry for the absolute values of the corresponding partial wave amplitudes e.g. in $\bar{2}40$ and 200 etc. in Fig. 10, however, some amplitudes have different signs so that due to the absorption the reflection profiles are different.

b) 71° Wedge

Experiments with the sharp wedge were done to show the consistency of the analysis and to deter-

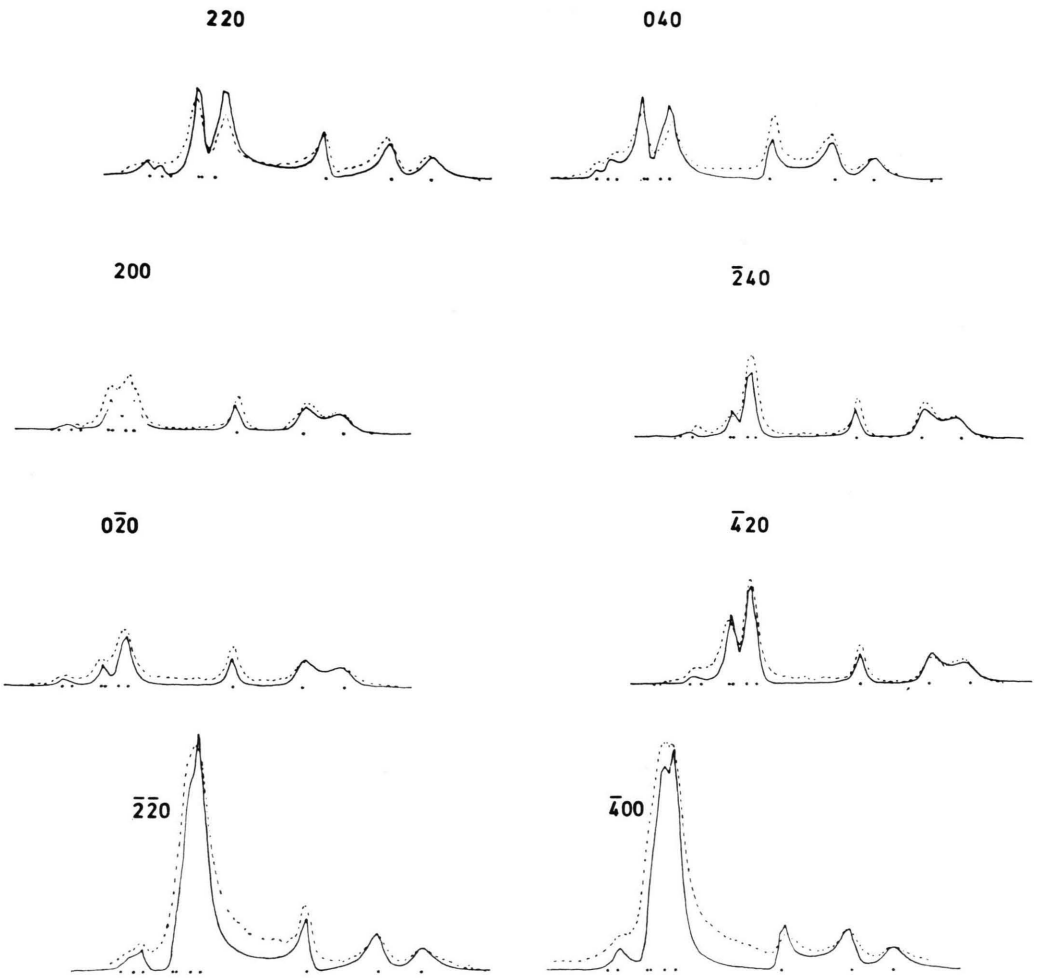

Fig. 11. Comparison of calculated (———) intensity distributions with photometer records (— — —) of the weak reflections near $G=-0.05$ and $H=2.0$ (condition (2) in Figure 3 a).

mine the structure potential V_{111}. The diffraction patterns for the two orientations (1) and (2) in Fig. 3 b were analysed. For these orientations the convergence of the many-beam approximation is not so good as for the blunt wedge. This depends on the higher density of atoms along the Ca-atom strings resulting in a higher potential. Because of this fact the Bloch wave at the Ca-atom strings is much more strongly concentrated, leading to a larger number of Fourier components which are necessary for a description of the density distribution. This can already be seen in the Kikuchi pattern taken at this orientation. The diffraction pattern shows much more reflections than that taken from the blunt-wedge experiment shown in Figure 4.

The density distributions in the different Bloch waves corresponding to the two orientations (1) and (2) are shown in Figs. 13 and 14 for $G=-1.75$, $H=0.0$ and $G=0.2$, $H=2.2$. As one can see the Bloch waves are more complicated than for the blunt wedge. Especially in Fig. 13 for case (1) in Fig. 3 b there does not exist the strong Bloch wave travelling only between the atom rows which is clearly excited in Fig. 14 for case (2). This Bloch wave (4) is not excited if $H=0$ i.e. if the incident electron beam lies in the (110) plane because of symmetry. For small deviations $\Delta H \neq 0$ from that orientation the Bloch wave (4) becomes more and more excited with increasing ΔH.

The diffraction pattern for $G=-1.75$ and $H=0.0$ [case (1) in Fig. 3 b) is shown in Figure 15. This pattern shows a symmetry with respect to the (110) plane, indicating that H is very near to zero. Since the intensity profiles of the pairs ($\bar{2}\bar{2}\bar{2}$,

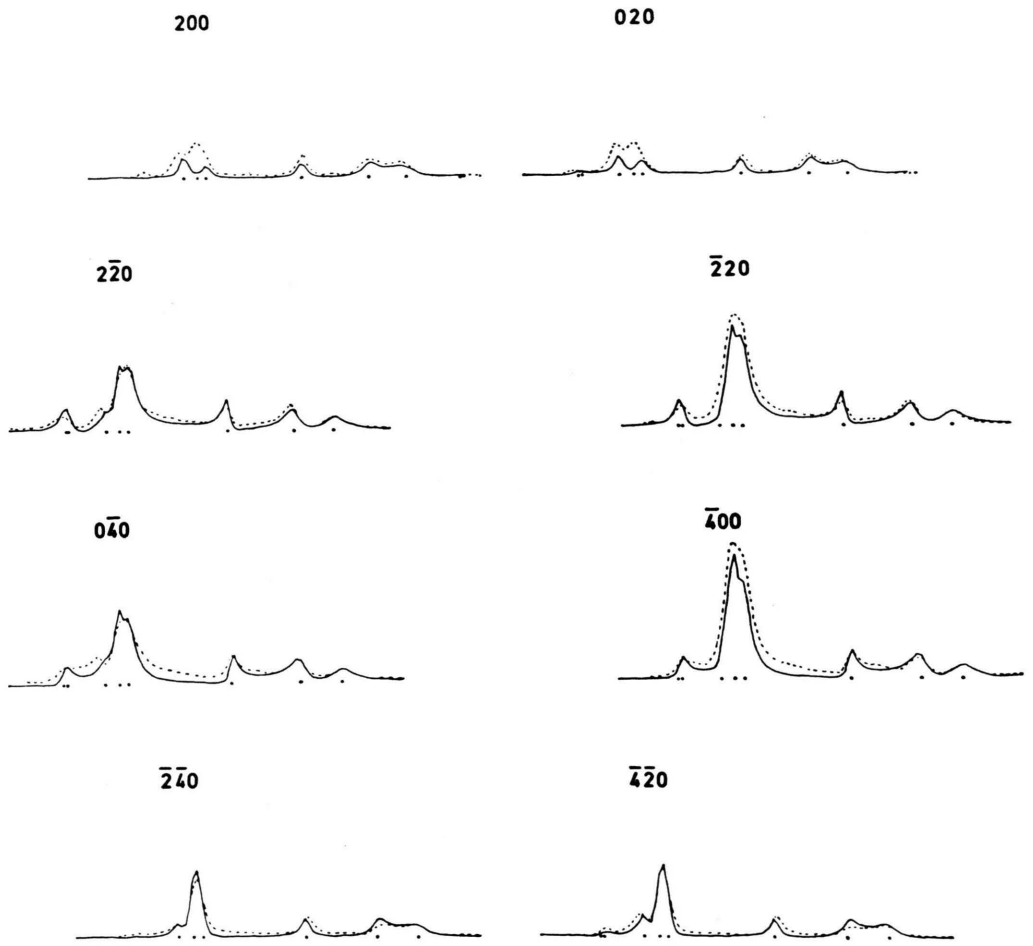

Fig. 12. Comparison of calculated (———) intensity distributions with photometer records (— — —) near $G=-2.025$ and $H=0.025$ (condition (3) in Figure 3 a).

$22\bar{2}$) etc. are nearly identical only one of the two reflections was compared with the calculated fine-structure profile. The comparison is shown in Fig. 16 where the superposition of 9 significant partial waves had been considered. No background was taken into account in the weak reflections. The agreement is not so good as in the blunt-wedge experiment. This may be due to the insufficient 50-beam approximation and to the neglect of background in the weak reflections which was not found to be so strong in the blunt-wedge experiment. The $00\bar{2}$ reflection has a strong background. The exposure time for the upper $00\bar{2}$ reflection was 1/5 from the exposure time for the lower reflection. The background intensity distribution in the $00\bar{2}$ reflection was nearly the same as in the strong excited reflections of the blunt-wedge experiment.

A similar background was found in 220 for the other orientation $G=0.2$ and $H=2.2$ corresponding to (2) in Figure 3 b. The comparison of the photometer records for this orientation with calculated fine-structure profiles is shown in Figure 17. The superposition of up to 14 partial waves had to be taken into account. The influence of background on the weak reflections is not so strong as in Figure 16. The strongly excited 220 beam shows only one strong peak with background. In this reflection the fine structure cannot be resolved because of the small differences between the eigenvalues (2), (3) and (4) and the influence of coherent overlapping.

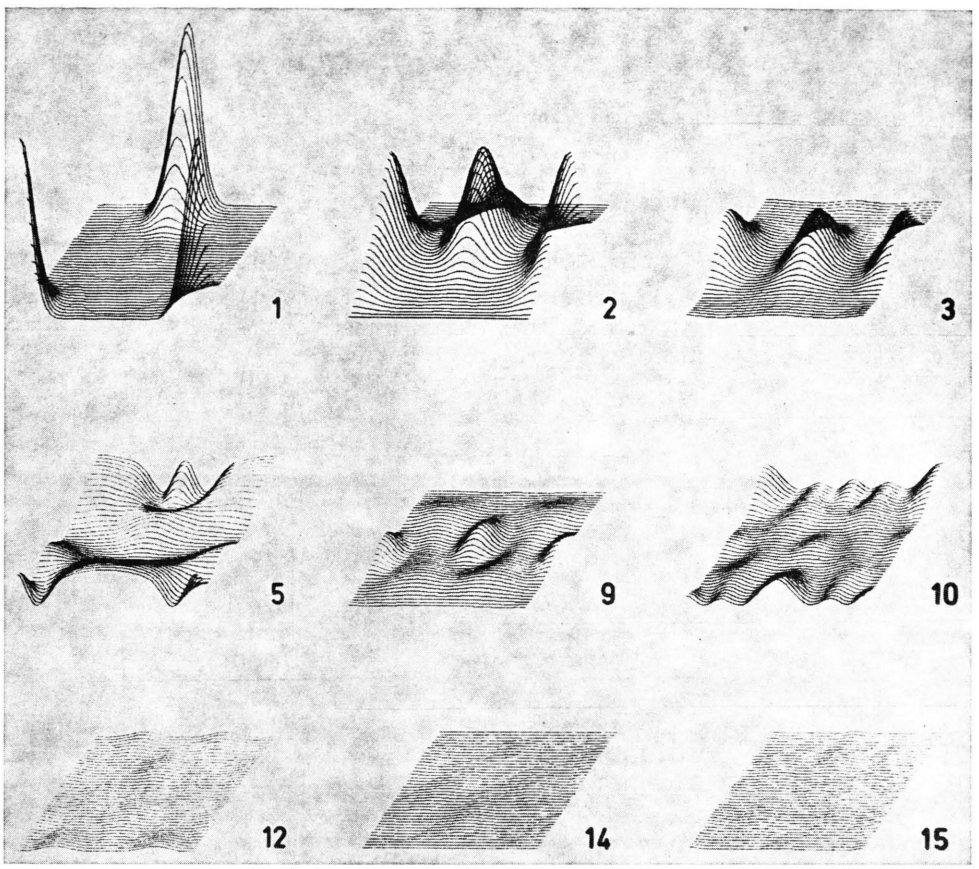

Fig. 13. Electron density distribution in the strong Bloch waves for the 71° wedge near $G=-1.75$ and $H=0.0$. The density distribution was calculated by a 42-beam approximation for the hatched area in Fig. 2 b (60 keV electrons).

§ 5. Discussion

a) Structure Potentials

By this analysis the low-indexed structure potentials and the absorption coefficients of strong Bloch waves were determined. In Table 1 the structure potentials are compared with theoretical values calculated from the atomic scattering amplitudes for neutral atoms and for ions, corrected to room temperature. The values for neutral atoms due to Doyle and Turner [9] and Cromer and Mann [11] do not differ very much. The structure potentials for ions are different for V_{200} and V_{220} while V_{111}, which depends only on Ca, shows only a small difference. For higher-indexed structure potentials the deviations between the values for ions and neutral atoms are very small. The experimentally determined structure potential V_{111} agrees within the experimental error with the theoretical values for atoms as well as for ions. However, the experimental value for the 200 structure potential is in agreement only with the value for ions. The 220 structure potential shows a remarkable deviation from the theoretical values which cannot be explained by the experimental error.

Table I. Structure potentials (in volts) of CaF_2 at room temperature; $B_{Ca}=0.6$, $B_F=0.8$ [10].

	Doyle, Turner [9] neutral atoms	Cromer Mann [11] neutral atoms	Cromer, Mann [11] Ca^{++} F^{--}	Exp.	Exp., 71° wedge, 50-beam approx.
V_{111}	4.97	5.00	4.91	4.95 ± 0.1	5.30
V_{200}	1.04	1.04	1.40	1.42 ± 0.1	1.55
V_{220}	5.57	5.56	5.48	5.75 ± 0.1	5.65

The structure potentials, determined from the experiments with the sharp and the blunt wedge, are in agreement if one applies a sufficiently accurate

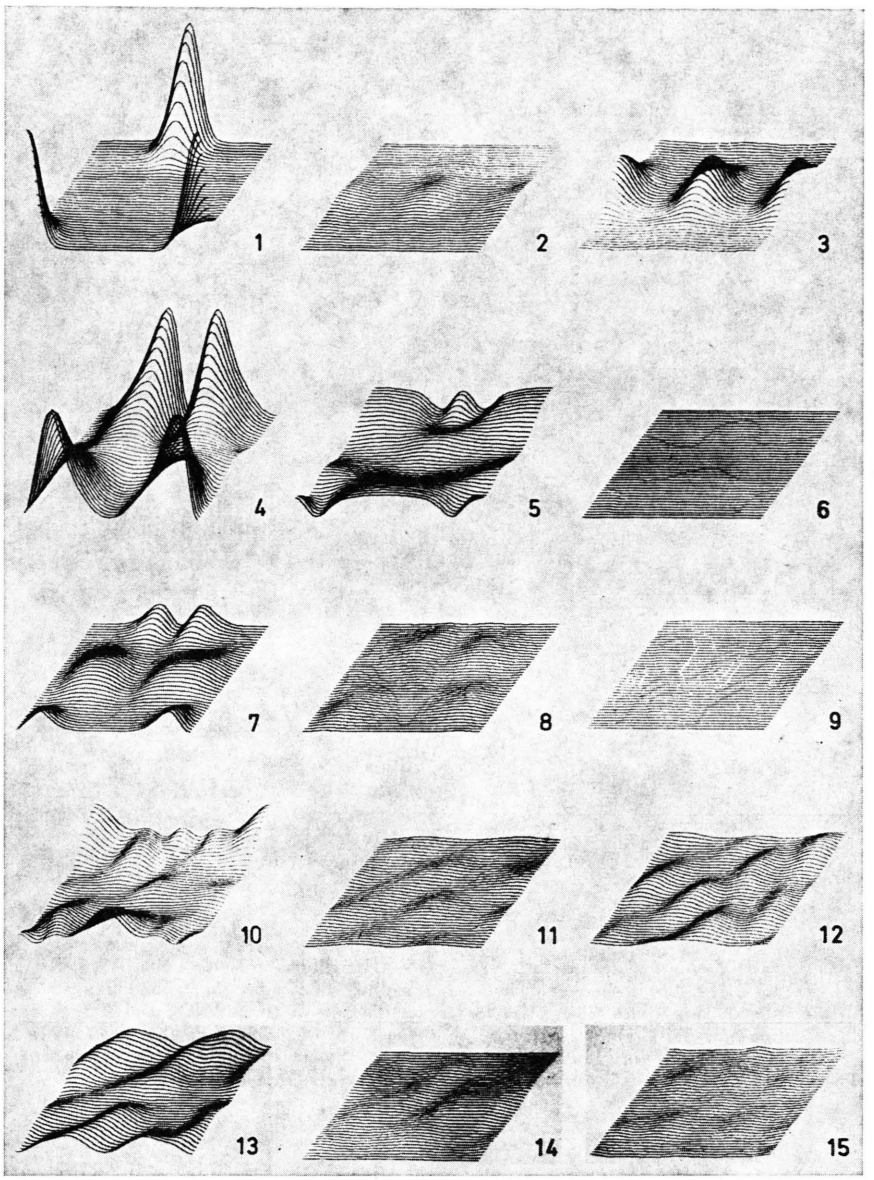

Fig. 14. Electron density distribution in the strong Bloch waves for the 71° wedge near $G=0.2$ and $H=2.2$. The density distribution was calculated by a 42-beam approximation for the hatched area in Fig. 2 b (60 keV electrons).

many-beam approximation for the analysis of the experimental data. For the sharp wedge the 50-beam approximation was not sufficient because the convergence of the many-beam approximation is very bad for that orientation as mentioned above. This was tested in the calculation by increasing the number of beams up to 152. The eigenvalue of Bloch wave (1), which is concentrated at the strings of Ca atoms, increased about 4.1%, going from the 50-beam approximation to the 152-beam approximation. The difference between 80 beams and 152 beams was still 1.4%. With the 50-beam approximation a structure potential of 5.3 volts was determined for 111. Also the other structure potentials V_{200} and V_{220} had to be changed to get agreement with the experiment. The structure potential V_{111} depends only on Ca, as one can see from the formula of the structure factor of CaF_2. In the insufficient 50-beam approximation one has to increase the effective 111 structure potential to take account of the strong con-

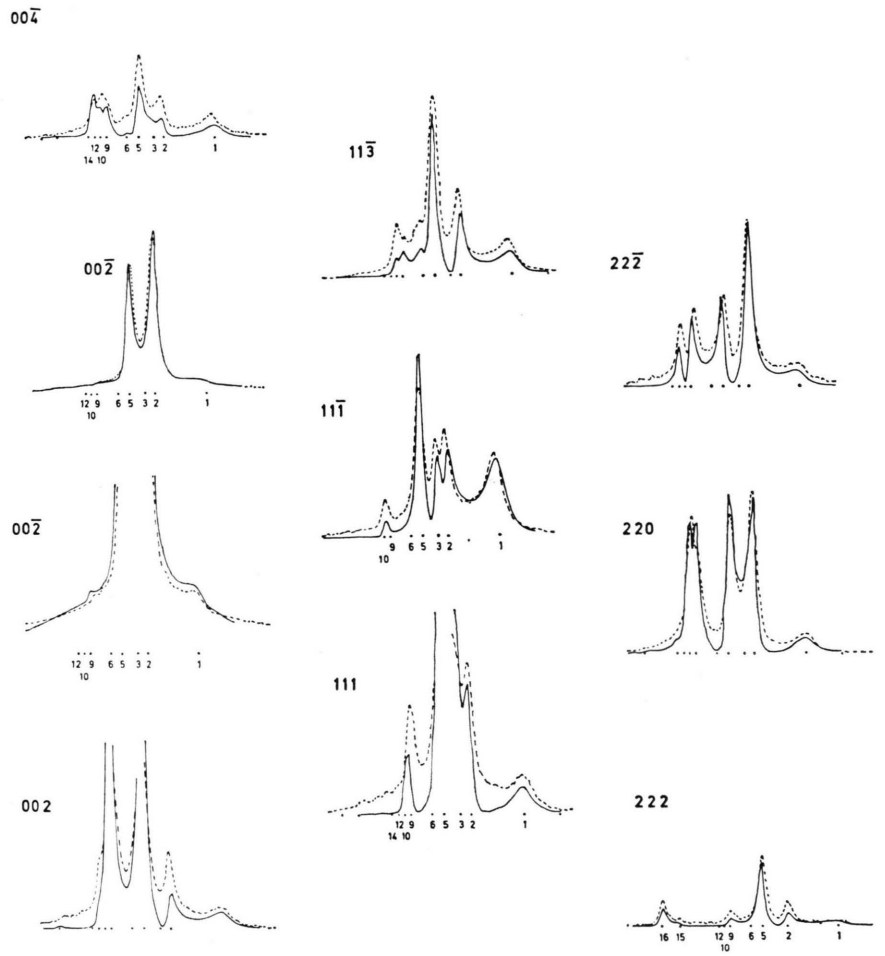

Fig. 16. Comparison of calculated fine-structure profiles (———) with photometer records of the diffraction pattern shown in Fig. 15 ($G=-1.75$, $H=0.0$) (— — —). The strong excited 00$\bar{2}$ reflection, showing a strong background, was recorded with two different exposure times. The lower 00$\bar{2}$ reflection was 5 times less exposed than the other reflections and the upper 00$\bar{2}$ reflection was 5.4 times less exposed than the lower 00$\bar{2}$ reflection, that is 27 times less than the other reflections. The difraction pattern shows a symmetry with respect to the (110) plane. This results in identical intensity profiles e.g. in 111 and $\bar{1}\bar{1}1$ etc. for H=0. From this reason only one reflection of a symmetric pair is plotted (condition (1) in Figure 3 b).

centration of Bloch wave (1) along the Ca-atom strings.

b) Absorption

In Table 2 the absorption coefficients for the different significant Bloch waves are shown for the 109° wedge and the 71° wedge. For the 109° wedge these absorption coefficients are valid for three characteristic orientations $G=2$, $H=0$; $G=0$, $H=2$ and $G=-2$, $H=0$. The electron density distribution in the Bloch waves for these orientations is the same as shown in Figure 8. For the analysis for the 109° wedge 9 Bloch waves had to be considered. [There exists a weak Bloch wave having the same eigenvalue as Bloch wave (3). These two Bloch waves were taken together and considered to be one Bloch wave labelled with number (3).] The values of the absorption coefficients are consistent if one considers the density distributions in the corresponding Bloch waves in Figure 8. Bloch wave (1) has the largest absorption coefficient, the one in Bloch wave (2) is smaller and in (3) there one has the smallest. The absorption coefficient of (4) is smaller than (1), but bigger than (3), and (5) is smaller than (4), smaller than (2), but bigger than (3) etc.

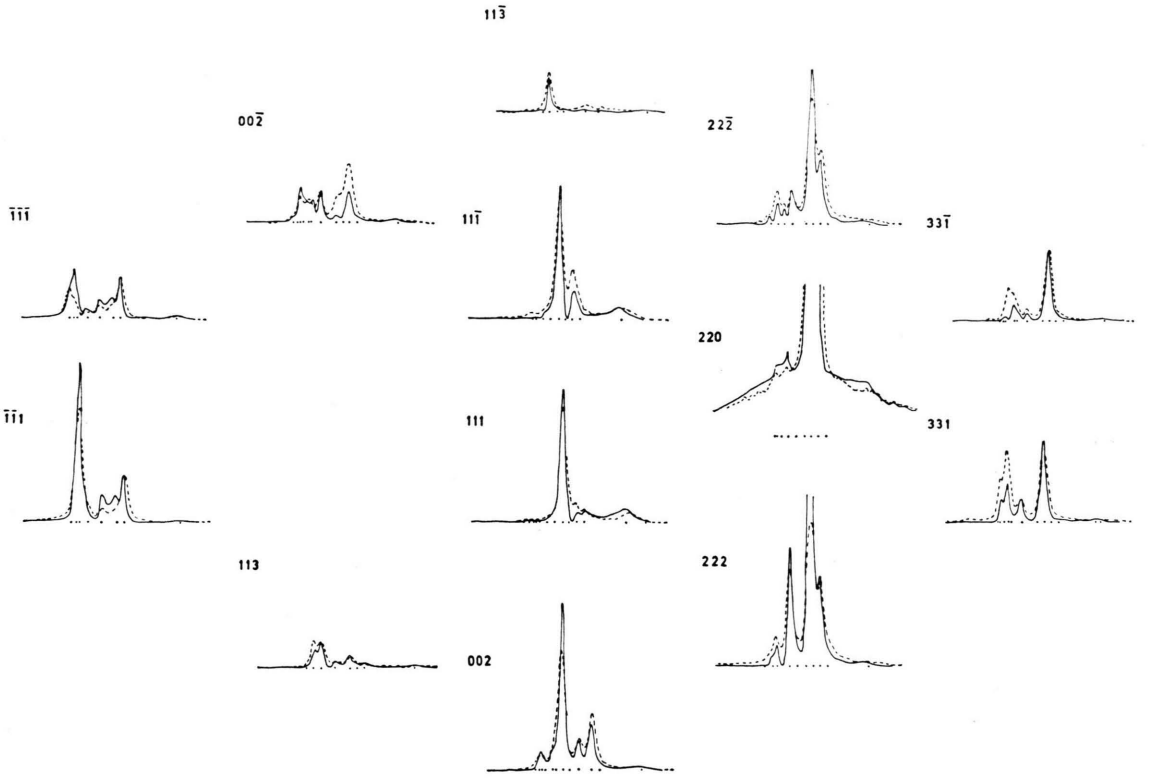

Fig. 17. Comparison of calculated fine-structure profiles (———) with photometer records (— — —) near condition (2) in Fig. 3 b at $G=0.2$ and $H=2.2$. In the excited 220 reflection a strong background can be seen.

With the sharp wedge different absorption coefficients were determined because the projection of the atoms on the plane perpendicular to the beam is different as was shown in Figure 2. In the [110] projection the density of the Ca atom along the atom rows is $\sqrt{2}$ times larger than in the [100] projection. This results in a larger potential along the rows as discussed above and consequently Bloch wave (1) is more strongly concentrated at the C-atom rows by which the inelastic interaction increases. The absorption coefficient for this Bloch wave increases as we see in Table 2. The density of the F atoms along the atom rows is smaller for this [110] orientation than for the [100] orientation. Correspondingly the potential of the atom rows is smaller, Bloch wave (2) is less concentrated and consequently the inelastic interaction is smaller, resulting in a smaller absorption coefficient for this Bloch wave shown in Table 2. Because of the higher density of atom strings in the projected area the absorption coefficients of the Bloch waves travelling between the atoms is larger than for the blunt wedge. The absorption coefficients for the sharp wedge are consistent if one considers the density distribution in the different Bloch waves in Figs. 13 and 14.

Table II. Absorption coefficients of significant Bloch waves for the blunt and sharp wedges.

	109° wedge		71° wedge	
		$G=-2$ $H=0$		$H=2$ $G=0$
n	10^3 Å^{-1}	10^3 Å^{-1}	n	10^3 Å^{-1}
1	11.0	18.1	1	18.0
2	8.0	7.0	2	7.0
3	4.0	7.0	3	7.0
	—	—	4	5.5
4	6.0	5.5	5	5.5
5	5.5	5.5	6	5.5
	—	—	7	4.5
6	4.5	—	8	5.0
	—	5.5	9	5.5
7	4.5	5.5	10	5.0
	—	—	11	6.0
	—	5.5	12	4.5
8	4.5	—	13	5.0
9	4.5	4.5	14	5.5

Bloch wave (4) in Fig. 13 has strong density maxima very near to the Ca-atoms rows. This con-

centration was not observed in the [001] projection (blunt-wedge experiment). The strong concentration is due to the higher string potential at the Ca-atom rows. Such increasing concentration is also observed in calculations with increasing accelerating voltage since the string potential along the atom rows becomes larger by the relativistic effect [12, 13]. It is clear that for a description of such sharp concentrations a large number of Fourier coefficients becomes necessary which leads to more and more beams which have to be taken into account in the many-beam approximation. This effect and the relation to band theory to overcome the difficulties is discussed in details by Kambe et al. [12].

§ 6. Summary

In this investigation it was shown that the diffraction pattern, obtained from a crystal wedge, can be described by the Bloch-wave picture, where the different Bloch waves are individually absorbed by the crystal. The intensity distributions in the different reflections are very sensitive to the orientation of the crystal and to the quality of the wedge faces. The good agreement between the observed and the calculated intensities due to Eq. (6) shows the sensitivity and the usefulness of the technique. The quality and the crystallographic orientation of the wedge faces could be estimated and determined from the diffraction pattern. The influence of a missing edge e.g. would have been detectable in the fine structures. During the investigations (112) cleavage faces near the edge were observed. By comparison of the diffraction pattern with a calculated intensity distribution it was found that some wedges were produced by a (112) and a (111) cleavage face. The diffraction pattern from undistorted wedges with (111) cleavage faces were easily reproducible.

From the Bloch-wave picture (e.g. Fig. 8) we understand that the diffraction patterns contain information on the crystal potential and on the absorption coefficients of the Bloch waves. The low-indexed structure potentials could be determined with good accuracy. While the structure potentials V_{111} and V_{200} are in good agreement with theoretical values for the ionized atoms, the 220 structure potential shows a remarkable deviation which cannot be understood.

The magnitude of the absorption coefficient of each Bloch wave depends on the electron density distribution in the Bloch wave; e.g. the Bloch wave which is concentrated along the rows of atoms, which act as centers of absorption, is most strongly absorbed. This model is supported by the results obtained with the two different wedges.

A more accurate analysis should take into account the scattering due to inelastic processes [16]. Such inelastic processes lead to the background in the diffraction pattern, which was taken into account only in the strong reflection by a Gaussian distribution as an integral effect. In the weak reflections, however, there is also a background, especially in the experiment with the sharp wedge, which should not be neglected. For a better understanding of the inelastic processes an analysis of these Bloch waves with a Möllenstedt energy analyser has been commenced [17].

We wish to thank Dr. K. Kambe for many stimulating discussions and Mrs. D. Schmidt-Barthmes for assistance during the analysis. K. Ishida wants to thank the Alexander-von-Humboldt-Stiftung for a scholarship and A. W. S. Johnson thanks the MPG and the CSIRO for financial support during his stay at the Fritz-Haber-Institut.

Appendix

Without absorption a Bloch wave (i) is given by

$$\psi_i(\boldsymbol{r}) = \sum_g \psi_g^{(i)} \exp 2\pi i(\boldsymbol{K}_g^{(i)} \cdot \boldsymbol{r}) . \quad (A\,1)$$

$\psi_g^{(i)}$ are the partial wave amplitudes, $\boldsymbol{K}_g^{(i)} = \boldsymbol{K}_0^{(i)} + \boldsymbol{g}$ the wave vectors in the crystal and $\boldsymbol{g}$ a reciprocal lattice-vector. With absorption this Bloch wave decays with increasing distance ξ from the entrance surface with an absorption coefficient μ_i as is shown schematically in Figure 5.

$$\psi_i'(\boldsymbol{r}) = \exp\left\{-\frac{\mu_i}{2}\cdot\xi\right\} \sum_g \psi_g^{(i)} \exp\{2\pi i \boldsymbol{K}_g^{(i)} \cdot \boldsymbol{r}\} . \quad (A\,2)$$

For convenience we introduce reduced wave vectors and reciprocal lattice vectors as in Reference 1.

The wave vectors are related to the eigenvalues τ_i by

$$\boldsymbol{K}_0^{(i)} = \frac{1}{\lambda}(\boldsymbol{S}_e + \boldsymbol{N}_e \cdot \tau_i) = \left(\frac{1}{\lambda}\right)\boldsymbol{S}_0^{(i)} \quad (A\,3)$$

with the vacuum wave-length λ, $\boldsymbol{S}_e$ a unit vector in the direction of the incident beam, and $\boldsymbol{N}_e$ a unit vector perpendicular to the entrance surface. In this notation, the eigenvalues τ_i are the normal-compo-

nent differences of the reduced wave vectors with respect to the normal component of $\boldsymbol{S}_e$. They are determined from the fundamental equations of the dynamical theory. With the reduced reciprocal lattice vector $\boldsymbol{B}_g = \lambda\, g$ other wave vectors can be expressed by

$$\boldsymbol{K}_g^{(i)} = \boldsymbol{K}_0^{(i)} + g = \frac{1}{\lambda}\,(\boldsymbol{S}_0^{(i)} + \boldsymbol{B}_g) = \frac{1}{\lambda}\cdot \boldsymbol{S}_g^{(i)}\,. \tag{A 4}$$

Without considering the absorption the eigenvalues τ_i are real. Usually the absorption is described by introducing complex potentials [7]. By the imaginary part of the potential the eigenvalues become complex

$$\tau_i = \tau_i' + i\,\tau_i''\,. \tag{A 5}$$

The imaginary part of the eigenvalue τ_i is related to the absorption coefficient μ_i, as one can see from (2) by replacing (5) in (3) and inserting (4) in (1), by

$$\mu_i = (4\pi/\lambda)\,\tau_i''\,. \tag{A 6}$$

If the exit surface of the crystal wedge is not perpendicular to the entrance surface the amplitude of a Bloch wave decreases on the exit surface with an absorption coefficient μ_{is} (s stands for Surface) which is related to μ_i by

$$\mu_{is} = \mu_i \cdot \sin\gamma \tag{A 6a}$$

as one can see from Fig. 5 (γ is the wedge angle). For a cube wedge the two absorption coefficients are equal.

[1] G. Lehmpfuhl and A. Reißland, Z. Naturforsch. **23 a**, 544 [1968].
[2] G. Lehmpfuhl, Z. Naturforsch. **27 a**, 425 [1972].
[3] G. Lehmpfuhl, Z. Naturforsch. **28 a**, 1 [1973].
[4] P. Goodman and G. Lehmpfuhl, Acta Cryst. **22** 14 [1967].
[5] M. v. Laue, Acta Cryst. **6**, 217 [1953].
[6] G. Lehmpfuhl and K. Molière, J. Phys. Soc. Japan **17**, Suppl. B-II, 130 [1962].
[7] K. Molière, Ann. Phys. Lpz. **34**, 461 [1939].
[8] R. Didszuhn, Thesis, FU Berlin 1969.
[9] P. Doyle and A. Turner, Acta Cryst. **A 24**, 390 [1968].
[10] V. W. Maslen, Proc. Phys. Soc. **91**, 466 [1967].
[11] D. T. Cromer and J. B. Mann, Acta Cryst. **A 24**, 321 [1968].
[12] K. Kambe, G. Lehmpfuhl, and F. Fujimoto, Z. Naturforsch. **29 a**, 1034 [1974].
[13] F. Fujimoto et al., Atomic Collisions in Solids, Vol. 2, Plenum Publ. Corp. New York, p. 547.
[14] C. J. Humphreys and R. M. Fisher, Acta Cryst. **A 27**, 42 [1971].
[15] A is about 5% of the intensity maximum of the 220 partial wave of Bloch wave (3), $\beta \approx 7\cdot 10^{-4}$ rad and $\alpha \approx 1\cdot 10^{-4}$ rad.
[16] K. Ishida and G. Lehmpfuhl, to be published.
[17] P. Fejes and G. Lehmpfuhl, 10th Intern. Conference of Crystallography, Amsterdam 1974. Acta Cryst. **A 31**, Part S, 251 [1975].